Resonance Raman Investigations of Cytochrome *c* Conformational Change upon Interaction with the Membranes of Intact and Ca^{2+}-Exposed Mitochondria†

Svitlana Berezhna,‡ Hartmut Wohlrab,§,|| and Paul M. Champion*,‡

Physics Department and Center for Interdisciplinary Research on Complex Systems, Northeastern University, 360 Huntington Avenue, Boston, Massachusetts, 02115, Boston Biomedical Research Institute, Watertown, Massachusetts 02472, and Department of Biological Chemistry and Molecular Pharmacology, Harvard Medical School, Boston, Massachusetts 02115

Received December 20, 2002; Revised Manuscript Received March 17, 2003

ABSTRACT: The conformational states of cytochrome *c* inside intact and Ca^{2+}-exposed mitochondria have been investigated using resonance Raman spectroscopy. Intact and swelling bovine heart and rat liver mitochondria were examined with an excitation wavelength (413.1 nm) in resonance with the Soret transition of ferrous cytochrome *c*. The different *b*- to *c*-type cytochrome concentration ratio in mitochondria from two different tissues was used to help assign the Raman spectral components. Resonance Raman spectra were also recorded for mitochondria fractions (supernatants and pellets) obtained from swollen (Ca^{2+}-exposed) mitochondria after differential centrifugation. The results illustrate that cytochrome *c* has an altered vibrational spectrum in solution, in intact, and in swollen mitochondria. When cytochrome *c* is released from mitochondria, its Raman spectrum becomes identical to that of ferrous cytochrome *c* in solution. The spectra of mitochondrial pellets indicate that a small amount of structurally modified cytochrome *c* remains associated with the heavy membrane fraction. Indeed, spectroscopic shifts in the low-frequency fingerprint and the high-frequency marker-band regions suggest that membrane binding leads to a partial opening of the heme pocket and an alteration of the heme thioether bonds. The results support the conclusion that most cytochrome *c* molecules in mitochondria are membrane-bound and that the cytochrome *c* structure changes upon binding. Furthermore, changes in the resonance Raman active mode located at 675 cm^{-1} in the spectra of intact, swollen, and fractionated mitochondria indicate that *b*-type cytochromes may also undergo structural alterations during mitochondrial swelling and disruption.

Cytochrome *c* is essential for normal functioning of living cells (*1*), and ironically, it also plays a key signaling role during the process of cell death (apoptosis) (*2*). In life and respiration, cytochrome *c* transfers electrons from cytochrome *c* reductase to cytochrome *c* oxidase (*1*). In apoptotic death, a key step in the initiation pathway is the translocation of cytochrome *c* from the mitochondrial membrane space into the cytosol (*2*). Numerous in vitro and in vivo studies have provided much information about the structure and the function of cytochrome *c* (*3*). Still, the precise physiological context of this protein in the living and dying cell remains poorly defined.

Cytochrome *c* is a six-coordinate low-spin heme iron species. The heme (iron protoporphyrin IX) has axial iron ligands at both the fifth and the sixth coordination positions: histidine (His18) and methionine (Met80) (*1*, *3*). In addition, two cysteine residues (Cys14 and Cys17) attach the heme to the protein via thioether bonds. The heme has only limited access to the surface of the protein. It lies within a crevice lined with hydrophobic amino acids. Only the edge of one pyrrole ring and the adjacent Cys17 thioether bond lie at the surface (*1*). Cytochrome *c*, which is located primarily at the outer face of the inner mitochondrial membrane (*1*) and its cristae (*1*, *4*), behaves as a peripheral protein (i.e., it can be removed from the membrane by relatively mild treatments such as changes in pH or ionic strength of the aqueous medium (*1*)). Nevertheless, the details of cytochrome *c* redox activity and its mechanism of membrane binding are clearly complex (*5*−*11*).

Cytochrome *c* catalyzes electron transfer from cytochrome *c* reductase to cytochrome *c* oxidase (two intrinsic inner membrane proteins) as well as between adjacent cytochrome *c* molecules (*12*). It also participates in redox cycles with cytochrome b_5, an outer membrane protein (*1*, *13*, *14*). Most interprotein electron-transfer reactions are preceded by the formation of reversible protein complexes that bring the interacting hemes into an almost coplanar alignment (*1*). Such an arrangement usually maximizes overlap between the electron wave functions of the interacting cytochromes. While a membrane bound cytochrome *c* can perform electron transfer between cytochrome *c* reductase and cytochrome *c* oxidase, it must also be available in an unbound conformation (*5*−*7*, *11*) to serve as an electron carrier from the inner membrane to the proteins bound in the outer membranes (e.g., with cytochrome b_5). Investigations of the interactions between cytochrome *c* and various membrane systems (*5*−*11*, *15*−*30*) suggest that mitochondrial cytochrome *c* is found in unbound as well as in several membrane-bound conformations, all of which are exchangeable (see earlier reviews, refs *6* and *8*).

† Supported in part by NIH DK35090 (P.M.C.), GM57563 (H.W.), and NSF MCB 0211816 (P.M.C.).

* Corresponding author. Telephone: (617) 373-2918. Fax: (617) 373-2943. E-mail: p.champion@neu.edu.

‡ Northeastern University.

§ Boston Biomedical Research Institute.

|| Harvard Medical School.

10.1021/bi027387y CCC: $25.00
Published on Web 05/01/2003

A recent model of cytochrome *c* interaction with the membranes and membrane proteins suggests that this complex dynamic process is controlled by interplay of electrostatic and hydrophobic binding forces. Cytochrome *c* interacts with the phospholipids of the inner mitochondrial membrane. This interaction yields at least two different cytochrome *c* conformations. One is created through electrostatic interactions of the positively charged cytochrome *c* with negatively charged phosphate groups of phospholipids (*5*−*7*, *22*−*24*). The other is created when cytochrome *c* partially embeds itself into the membrane bilayer through hydrophobic interactions (*22*−*24*, *28*, *29*). The interaction of cytochrome *c* with the various redox protein partners potentially yields additional conformations (*3*, *5*, *31*).

The existence of multiple membrane-bound conformations of cytochrome *c* in mitochondria has been verified in studies of the two step release of cytochrome *c* from isolated rat liver mitochondria (*32*). First, the interaction between cytochrome *c* and its membrane-anchoring associate cardiolipin must be disrupted to generate a pool of soluble cytochrome *c*. Thereafter, permeabilization of the outer membrane leads to the significant release of cytochrome *c*. It was demonstrated that solubilization of the two bound cytochrome *c* conformations requires different detachment stimuli (*32*). The electrostatically bound conformation is sensitive to ionic strength, surface-charge density, or pH, while hydrophobically bound conformations respond to a disturbance of the membrane structure or modification of the mitochondrial lipids, specifically, cardiolipin.

More support for the view of different binding environments for cytochrome *c* comes from investigations of mitochondrial cristae modifications during apoptosis (*4*). On the basis of the results of combined high-voltage electron microscopic tomography (HVEM) and biochemical measurements, Scorrano and co-workers (*4*) concluded that a major part of cytochrome *c* in mitochondria is separated from the intermembrane space and is stored in cristae. These results are in good agreement with earlier functional estimates of Bernardi and Azzone (*11*), which suggest that only 15−20% of cytochrome *c* is in the intermembrane space.

Interestingly, through recognition of different conformations of cytochrome *c* in apoptotic and necrotic T hybridoma cells with monoclonal antibodies, it was shown that the cytochrome *c* conformation, which activates apoptosis in these cells, is membrane bound (*23*). Specifically, immunofluorescence confocal microscopy revealed that conformationally altered cytochrome *c* in post-apoptotic T hybridoma cells remains associated with mitochondria. Moreover, the heavy membrane (mitochondria containing) fraction of post-apoptotic, but not of live cells, was functional in caspase activation. The supernatant of post-apoptotic mitochondria did not show a pro-apoptotic function. On the basis of these observations, it was suggested that the membrane-bound cytochrome *c* may be the relevant caspase coactivation factor in apoptosis. Involvement of membrane-bound cytochrome *c* in apoptosis appears contradictory considering that cytochrome *c* must interact with Apaf-1, dATP, and procaspase-9 in the cytosol to form an apoptosome (*2*). To resolve this issue, a more precise understanding of the possible mechanisms for cytochrome *c* translocation to cytosolic states is required.

Despite extensive work on the problem of cytochrome *c* binding, it remains unclear what kind of reorganizations the structure of native cytochrome *c* undergoes when the protein associates with the membrane and whether the protein's structure pronouncedly differs depending on the type of binding (i.e., electrostatic or hydrophobic).

In the investigation described here, we use resonance Raman spectroscopy to examine the conformational states of cytochrome *c* in its native environment inside mitochondria. Vibrational spectroscopy has been recognized to be a sensitive tool, capable of revealing subtle changes in the molecular structure of proteins. The difficulty of applying this method to the complex mitochondrial system arises from the presence of several different heme proteins (*1*). Because the peaks of the electronic absorption bands of *c*- and *b*-type cytochromes are quite similar, it is difficult to resonantly enhance only one type of cytochrome in whole mitochondria. Nevertheless, this obstacle can be resolved by taking advantage of clear differences in the Raman marker bands of the purified *c*- and *b*-type cytochromes (*33*−*35*). In earlier work, Adar and Erecinska (*36*) obtained resonance Raman spectra of whole pigeon breast mitochondria using Q-band excitation (520.8, 530.9, and 568.2 nm). The results reported by these authors lack the low-frequency part of the spectra (below 600 cm^{-1}), which is important for identification of the axial heme ligands. Even so, they were able to conclude that the biochemical states of the hemes and/or their protein environments in the intact mitochondria are different from the native protein conformations in solution. Here, we use Soret-band excitation (413.1 nm) to obtain the resonance Raman spectra of mitochondria from two types of tissue (bovine heart and rat liver) under different physiological conditions. To obtain additional information on the putative structural changes of cytochrome *c* on/in mitochondrial membranes, data were collected from both intact mitochondria and mitochondria that were induced to swell and release cytochrome *c*. The observed differences are discussed in the context of interactions between the cytochromes and the mitochondrial membrane.

MATERIALS AND METHODS

Preparation of Rat Liver and Bovine Heart Mitochondria. Rat liver mitochondria were prepared by standard centrifugation procedures (*37*) in MSH (210 mM mannitol, 70 mM sucrose, 5 mM HEPES,[1] pH 7.5) buffer supplemented with 1 mM Na_2EDTA and 0.1% BSA. The last washing was performed in an EDTA-free medium, and final mitochondria were suspended in MSH buffer without EDTA at 96 mg of protein/mL. Fresh mitochondria were used within 4 h. Bovine heart mitochondria were prepared in MSE (220 mM mannitol, 70 mM sucrose, 0.2 mM EDTA, pH 7.2) buffer as described earlier (*38*) and stored at 40 mg of protein/mL (−20 °C). The frozen mitochondria were rapidly thawed and used within 3 h.

For experiments with mitochondria swelling and release of cytochrome *c*, the original medium was substituted with KCl buffer (150 mM KCl, 5 mM Tris-HCl, pH 7.4) and 200 nmol of Ca^{2+} per mg of protein was added in the presence

[1] Abbreviations: EDTA, ethylenediaminetetraacetic acid; HEPES, *N*-2-hydroxyethylpiperazine-*N*′-2-ethanesulfonic acid; UV, ultraviolet; BSA, bovine serum albumin; Pi, inorganic phosphate.

of 5 mM Pi. A buffer with 150 mM KCl is a standard medium for detaching loosely bound cytochrome *c* from the inner membrane (*22*). About 3 h after Ca^{2+} overload, the mitochondrial suspensions were centrifuged at 9800*g* for 5 min at 4 °C. It was demonstrated (*22*) that this protocol washes electrostatically bound cytochrome *c* from the mitochondrial intermembrane space. Supernatants were additionally filtered through a 0.22 μm filter (Millex-GV) that allows soluble proteins but not mitochondrial fragments to pass through. The resulting supernatants and pellets were used for measurements of Raman and absorption spectra. All samples were measured in sealed square quartz cuvettes with a 3 mm optical path (NSG Precision Cells). The mitochondrial samples remained reduced at the protein concentration used.

Cytochrome c. Horse heart cytochrome *c* was purchased from Sigma and dissolved in 100 mM sodium phosphate buffer (pH 7.2). The sample was reduced with ascorbic acid.

Raman Spectroscopy. All resonance Raman measurements were carried out at 413.1 nm (krypton ion laser, Coherent Innova 300) in a 90°-scattering geometry using a *Spex1870* spectrometer (2400 grating, 0.5 m focal length, slit width 100 μm). The output of the monochromator was coupled to a CCD detector cooled by liquid nitrogen (Princeton Instruments, Inc.). The experimental setup also includes focusing and collection optics and a holographic notch filter (Kaiser Optical system). A commercial software (Princeton Instruments, Inc.) provided elimination of the noise spikes in the spectra caused by cosmic rays. The average power at the sample was 12−15 mW for whole mitochondria and 5 mW for cytochrome *c* in solution. Signal-to-noise ratio was improved by several repetitive scans at a rate of 30 s exposure per scan (1 scan covers the spectral region of ~800 cm^{-1}). The spectra were calibrated using neat fenchone. The accuracy of absolute frequencies was ± 1 cm^{-1} and less than ± 0.2 cm^{-1} for relative shifts of bands. Collection of a typical spectrum took 2 min. Sample integrity was monitored by UV/visible spectroscopy before and after each resonance Raman experiment.

UV and Visible Spectra. UV and visible spectra were recorded with a Hitachi U-3410 spectrophotometer.

RESULTS

The aim of this work is to explore vibrational spectra of cytochrome *c* in real time during the course of mitochondrial swelling and upon its release from disrupted membranes. We prepared mitochondria from rat liver and bovine heart, which represent tissues having different functions and which also vary in structure and in cytochrome content. Liver mitochondria contain relatively few cristae and thus have more matrix space and less inner membrane surface than heart muscle mitochondria. The heart mitochondria lack many of the enzymes found in liver mitochondria, their cristae are packed more densely, and less matrix space is available (*1*). Heart mitochondria are thought to possess more of the tightly membrane-bound cytochrome *c*. Likewise, the shape and volume of cristae can be expected to affect the diffusion of cytochrome *c* between intracristal and intermembrane compartments, as well as the fraction of cytochrome *c* bound to the inner membrane (*39*). Both liver and heart mitochondria were investigated because, in addition to the differences in cristae, they contain different relative concentrations of the various cytochromes, which helps in the assignment of the resonance Raman peaks.

The choice of 413.1 nm as an excitation wavelength provides conditions for a preferential resonant enhancement of low-frequency Raman modes of reduced cytochrome *c* because the absorption peak of its Soret band is at 415 nm. Nevertheless, one might also expect contributions to the Raman spectra (especially in the high-frequency region) from the reduced *b*-type cytochromes, which have Soret band maxima at 424, 430, and 432 nm, respectively, for b_{560}, b_{562}, and b_{566} (inner membrane proteins) and at 423 nm for b_5 (outer membrane protein). Estimates of the cytochrome content of the mitochondria from these two tissues are as follows (*1*): bovine heart mitochondria 0.75 μmol of cytochrome $c + c_1$ per gram of protein and 0.5 μmol of cytochrome *b* per gram of protein; rat liver mitochondria 0.11 μmol of cytochrome $c + c_1$ per gram of protein and 0.1 μmol of cytochrome *b* per gram of protein. The concentration ratio of cytochrome $c + c_1$ to cytochrome *b* is 1.5:1 for bovine heart and 1:1 for rat liver. The preparations that we used had, respectively, in the bovine heart mitochondria 30 μM cytochrome $c + c_1$ and 20 μM cytochrome *b* and in the rat liver mitochondria 10.6 μM of cytochrome $c + c_1$ and 9.6 μM cytochrome *b*. We anticipated that the different cytochrome ratios found in rat liver and bovine heart mitochondria could aid in the interpretation of the Raman spectra obtained at 413.1 nm. In the Discussion, we assume that the strongest enhancement occurs for ferrous cytochrome *c*. Possible interference from *b*-type cytochromes is taken into account.

Raman Spectra of Intact Mitochondria. Figure 1a,b shows the low and high-frequency resonance Raman spectra for intact reduced mitochondria from bovine heart and rat liver, along with the spectra of reduced cytochrome *c* in solution. The fluorescence background signal is not conducive to obtaining well-resolved spectra from mitochondria. Spectra obtained by Adar and Erecinska (*36*) of pigeon breast mitochondria with visible excitation also exhibit fluorescence contamination. For a given set of experimental conditions (e.g., 15 mW laser power at the sample and averaging the final spectra over 4 scans of 30 s each), we observed a better signal-to-noise ratio for bovine heart mitochondria, which can be explained by the higher concentration of cytochromes in this sample and by the absence of fluorescent liver enzyme systems such as cytochrome P-450. Although this enzyme system is present in rat liver mitochondria in minor amounts as compared to other cytochromes (0.011 μmol/g of protein (*1*)), fluorescence from the flavoproteins associated with the cytochrome P-450 system may not be negligible. The mode at about 490 cm^{-1} (Figure 1a) arises from the quartz cuvette. Because of the poor optical quality of the samples (mitochondrial solutions are strongly opaque media), we aligned the excitation beam very close to the wall of the cuvette; thus, the low-frequency region of almost all spectra contain a trace of the quartz peak. To verify the reproducibility of the data, we repeated the measurements seven times for bovine heart and five times for rat liver mitochondria and obtained similar results.

Raman Spectra of Swelling Mitochondria. The introduction of Ca^{2+} ions leads to accumulation of calcium diacetate in the mitochondrial matrix and subsequent osmotic swelling

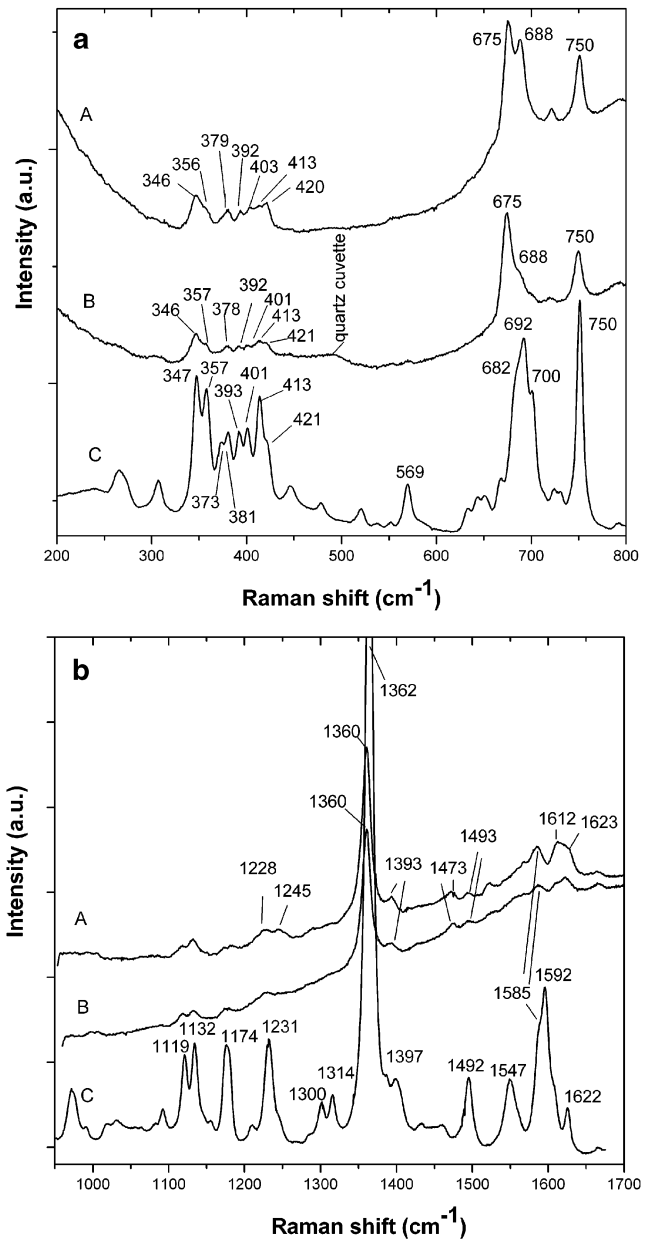

FIGURE 1: Soret resonance Raman spectra of intact bovine heart (A) and rat liver (B) mitochondria obtained with 413.1 nm excitation in the low (a) and high (b) frequency regions along with the spectrum of ferrous cytochrome *c* in a buffer solution (C). In the spectrum of native cytochrome *c*, the peak position of ν_4 mode (cut off in the plot (C)) is at 1362 cm^{-1}.

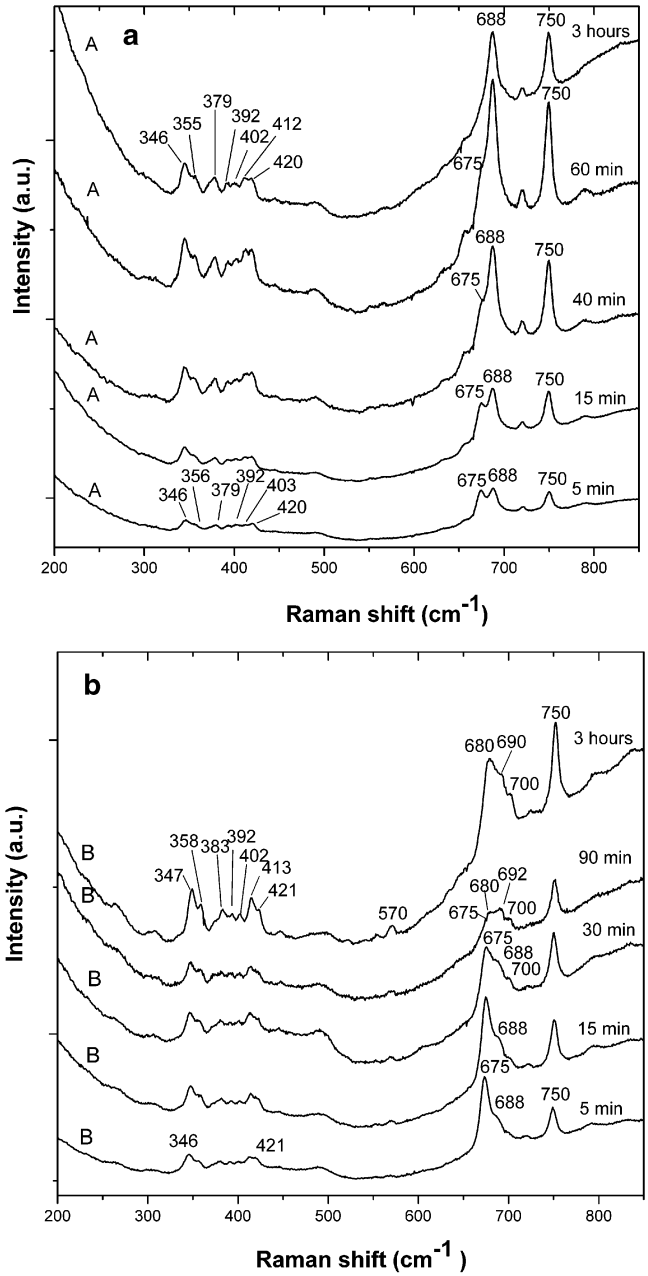

FIGURE 2: Time evolution of Soret resonance Raman spectra in the low-frequency region of bovine heart (a) and rat liver (b) mitochondria loaded with Ca^{2+}. Spectra were obtained with 413.1 nm excitation at indicated time intervals.

proportional to the extent of Ca^{2+} uptake (*1*). In both mitochondrial preparations, the original isolation media were substituted with high ionic strength KCl buffer, and Ca^{2+} was added in the presence of Pi to induce mitochondria swelling. The rationale of these experiments was to induce changes in the Raman spectra of the mitochondria, which undergo swelling and release cytochrome *c* into the extramitochondrial medium. It is expected that cytochrome *c* undergoes structural alterations during this process, specifically, a conversion from membrane-bound to soluble conformation, and we attempted to monitor these changes. The results obtained for bovine heart and rat liver mitochondria loaded with Ca^{2+} are shown in Figures 2 and 3. During the first 30−40 min after Ca^{2+} addition, we observed significant changes in the vibrational spectra in the region near 700 cm^{-1}. Specifically in the case of rat liver mitochondria, we observed a decrease in the relative intensity of the 675 cm^{-1} band (after about 1 h at 4 °C the band at 675 cm^{-1} became undetectable) and an emerging triplet structure between 680 and 700 cm^{-1}. In contrast, the triplet structure was not revealed in bovine heart mitochondria, but a sharp peak at 688 cm^{-1} appeared. At the same time, the spectra in the 300−500 cm^{-1} low-frequency region became more complex and evolved toward the 8-peak structure, which is a unique feature of soluble cytochrome *c*.

The data that we were able to record in the high-frequency part of the Raman spectrum (above 900 cm^{-1}) suffer from a strong fluorescence background (Figure 3). We collected data scans within ~20 min intervals for 4 h (the samples were kept at 4 °C during signal acquisition), and after the runs both sample preparations were centrifuged. The resulting

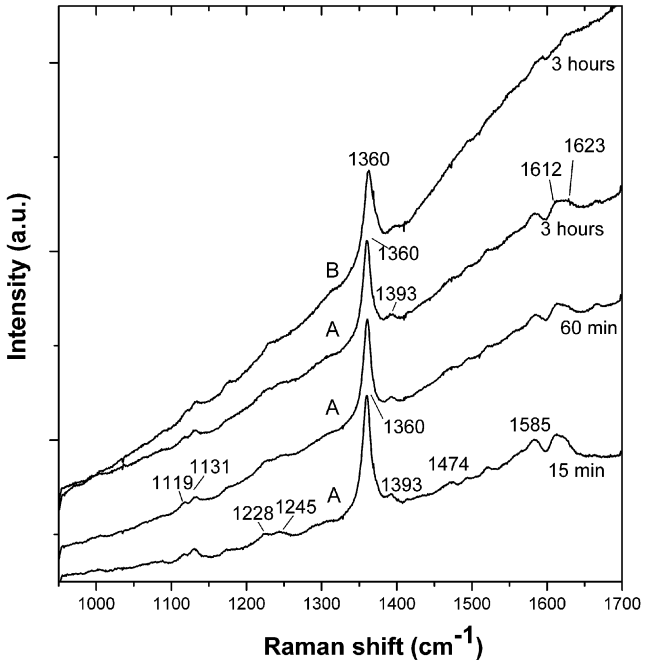

FIGURE 3: Time dependence of Soret resonance Raman spectra in the high-frequency region of bovine heart (A) and rat liver (B) mitochondria loaded with Ca^{2+}. Spectra were obtained with 413.1 nm excitation at indicated time intervals.

supernatants and pellets were probed independently, and the Raman spectra are shown in Figures 4 and 5, respectively. The spectrum, which we obtained for supernatants of swollen mitochondria (Figure 4a,b) corresponds to that of native cytochrome *c*, while the pellets of swollen mitochondria (Figure 5a,b) show a spectrum resembling that of intact mitochondria and differing from that of soluble cytochrome *c*. In addition to the Raman spectra, we also recorded the absorption spectra for supernatants of both rat liver and bovine heart mitochondria as seen in Figure 6, where they can be compared with the absorption spectrum of reduced cytochrome *c* in buffer solution.

DISCUSSION

The structural changes that cytochrome *c* undergoes upon binding to model membrane systems (polyanions, phospholipid vesicles, electrodes) have been investigated using a variety of biophysical techniques including resonance Raman spectroscopy (*17*, *18*, *40*, *41*), ^{1}H, ^{13}C, ^{31}P nuclear magnetic resonance (*15*, *16*, *42*), circular dichroism (*43*), and other spectroscopic and biochemical techniques (*44*−*47*). According to these studies, cytochrome *c* undergoes a wide range of conformational changes upon association with the model membranes. Generally, these studies demonstrated that binding of cytochrome *c* to model membrane systems creates a protein conformation with a destabilized tertiary structure but a nativelike helical secondary structure and a more open heme pocket as compared to the native protein. Electrostatic (or loose) binding of cytochrome *c* to the membrane does not yield significant changes in the protein conformation as shown by circular dichroism (*43*) and resonance Raman measurements (*40*, *41*). The hydrophobic (or tight) interaction between the protein and the phospholipids, however, leads to protein penetration into the membrane bilayer and a partial loss of α-helical structure (*22*−*27*). Since protein−phospholipid interactions are considered to be a close simulation of the putative interaction of cytochrome *c* with the inner mitochondrial membrane (*48*), the structural information reported in the studies with artificial membranes is likely to hold also for cytochrome *c* inside mitochondria. However, support for this concept from a direct analysis of cytochrome *c* in the functioning mitochondrial membrane in situ is lacking.

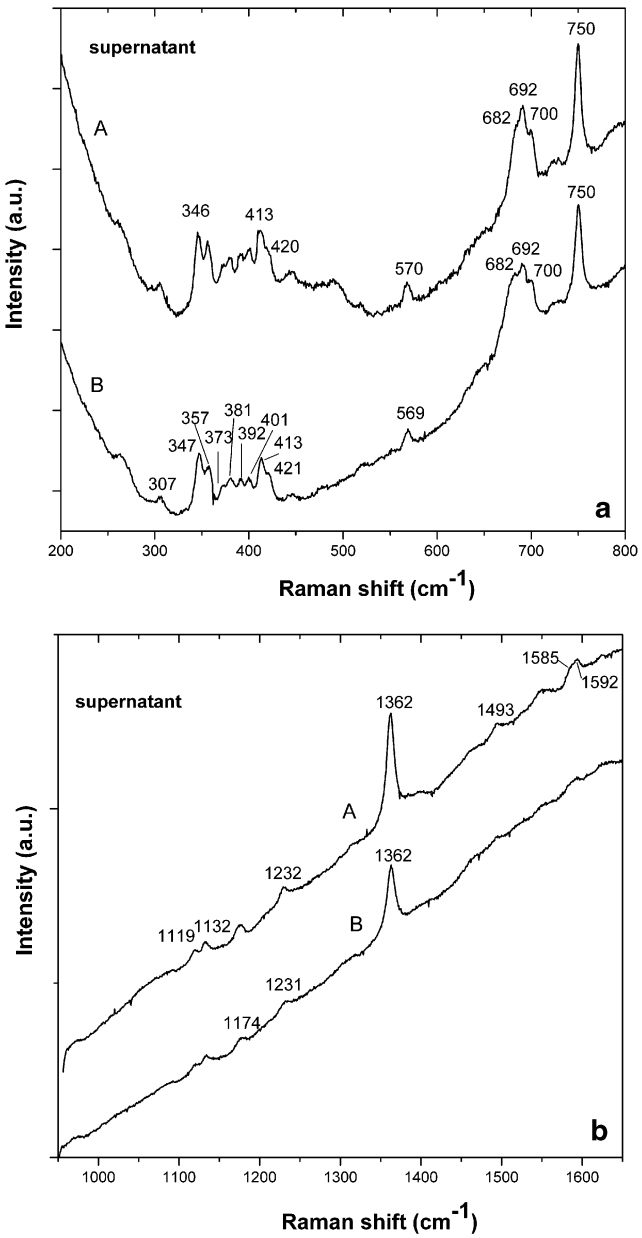

FIGURE 4: Soret resonance Raman spectra in the low (a) and high (b) frequency regions of bovine heart (A) and rat liver (B) mitochondria supernatants. Spectra were obtained with 413.1 nm excitation.

The structures of heme proteins in general (*49*) and of cytochrome *c* in particular (*50*) have been scrupulously correlated with the frequencies of certain resonance Raman modes. The low-frequency region (∼200−800 cm^{-1}) is informative for identification of the heme structural inhomogeneity and the axial ligation of the central iron atom. The high frequency or marker-band region (1300−1700 cm^{-1}) reveals the oxidation (ν_4), spin, and coordination state (ν_2, ν_3) of the heme iron atom. All of these frequencies

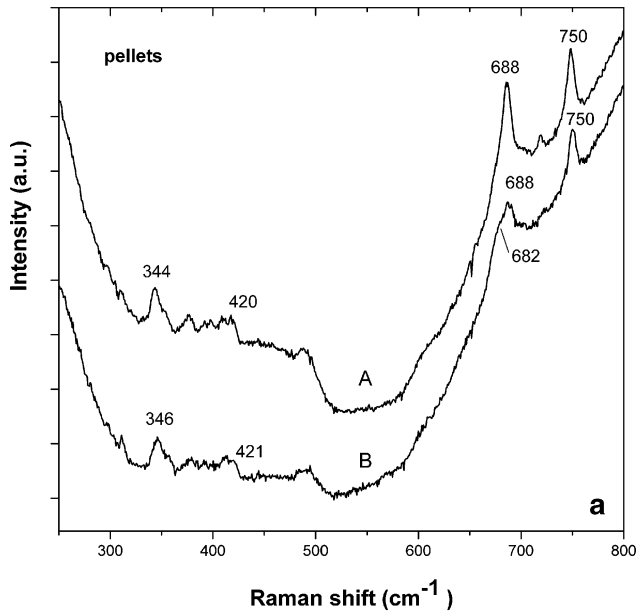

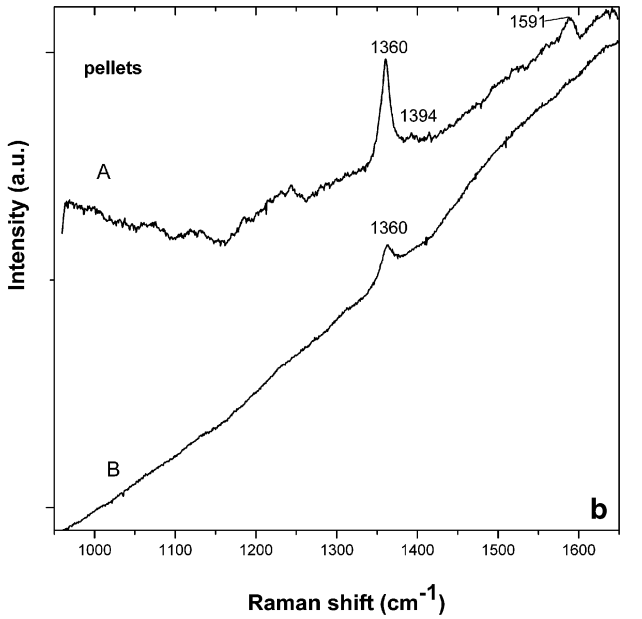

FIGURE 5: Soret resonance Raman spectra in the low (a) and high (b) frequency regions of bovine heart (A) and rat liver (B) mitochondria pellets. Spectra were obtained with 413.1 nm excitation.

correspond to skeletal vibrations of the porphyrin. The modes ν_{10} and ν_{19} also reflect the spin and coordination (5 or 6) state of the metal atom. These general rules apply to cytochrome *c*, but specific differences (relative to protoporphyrin IX) occur because of the existence of two covalent bonds $-CH(SR)CH_3$ at the 2 and 4 positions in the porphyrin ring (*1*, *3*, *50*), which attach the heme to the polypeptide chain through two thioether bridges. The symbol R represents cysteine residues Cys14 and Cys17 in the 2 and 4 positions, respectively. The notation here is adopted from the paper by Hu and co-workers (*50*), who provided complete assignment of cytochrome *c* resonance Raman spectra, using cytochrome *c* reconstituted with isotopically labeled hemes. At the 6 and 7 positions (*50*) in the porphyrin ring, cytochrome *c* has two propionate groups, whose vibrations are also Raman active. Band frequencies are almost the same

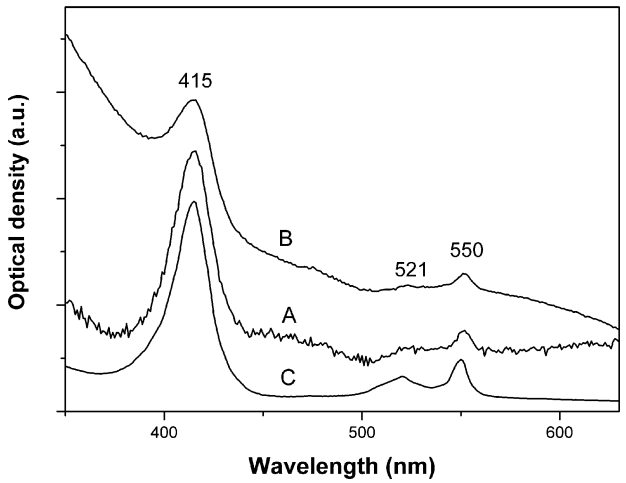

FIGURE 6: Absorption spectra of cytochrome *c* released from swollen bovine heart (A) and rat liver mitochondria (B) as well as of ferrous cytochrome *c* in buffer solution (C). Absorption spectrum of ferrous cytochrome *c* is downscaled by a factor of 9.

for ferric and ferrous cytochrome *c*, except for the high-frequency skeletal modes, which reflect the different extent of back-bonding (*50*). The relative intensities of the Raman modes for Fe^{2+} and Fe^{3+} cytochrome *c* species are also very similar, reflecting the minimal change in heme structure in the two oxidation states (*50*).

In general, the resonance Raman spectra of intact reduced mitochondria excited at 413.1 nm do not exactly replicate the spectrum of the native reduced cytochrome *c* (Figure 1a,b). The mitochondria spectra display a complex pattern of bands, only some of which belong to reduced cytochrome *c*. A comparison of the spectra of the purified protein with the spectra of mitochondria reveals that mitochondria have new bands that are not spectral features of cytochrome *c* (e.g., 675, 1228, 1245, 1473, 1568, 1612, and 1622 cm^{-1}. Also, the 1362 and the 1397 cm^{-1} bands of cytochrome *c* are downshifted in mitochondria spectra to 1360 and 1393 cm^{-1}, respectively, and the 1300, 1314, 1547, and 1592 cm^{-1} modes of cytochrome *c* are not detected at all. On the other hand, the spectra obtained for bovine heart and for rat liver mitochondria show good agreement of their peak positions, although not all of the bands are equally enhanced in both spectra.

Low-Frequency Region. Low-frequency vibrational modes in the cytochrome *c* Raman spectrum create a unique eight-peak structure of closely spaced bands that clearly distinguishes cytochrome *c* from other heme proteins (*49*, *50*). The number of vibrations is doubled as compared to other heme proteins and is considered an indicator of a closed heme crevice and a pronounced saddling distortion of the heme group in cytochrome *c* resulting from the six-coordinate state and the existence of strong steric constraints on the heme (*40*, *41*, *50*). The characteristic four sets of doublet bands, clustered in the spectral region ~330−430 cm^{-1}, are assigned to the two porphyrin stretching modes ν_8(347 cm^{-1}) and ν_{50}(357 cm^{-1}), and the remaining three pairs are, respectively, C−C−C and C−C−S bending modes of the propionate (at the 6,7 positions) and thioether (at the 2,4 positions) groups (*50*).

In both of the intact mitochondria samples, the peak positions in the ~330−430 cm^{-1} region are well-correlated

with cytochrome *c* modes (Figure 1a), but the spectra lose their resolution, and a prominent octet is not clearly observed. The same effect was observed by Hildebrandt et al. (*17*, *18*, *40*, *41*) when cytochrome *c* was bound to an artificial membrane interface. This was explained as a consequence of a looser structure around the heme crevice in the membrane-bound protein, which could also be associated with weakening of the Fe−Met80 bond (*17*, *18*) and/or a partial unfolding of the protein (*51*). When the protein is bound to the membrane, the tertiary structure and axial ligand interactions of the heme are relaxed (*15*−*18*), and as a consequence, the spectral pattern is inhomogeneously broadened. The effect is stronger for bovine heart mitochondria, which may be related to the higher fraction of membrane-bound cytochrome *c* in this sample (because of dense packing of the inner membrane cristae). A careful inspection of the mitochondria and cytochrome *c* spectra reveals small (∼2 cm^{-1}) frequency differences for some of the low-frequency bands. While in the case of well-resolved and/or isolated peaks these differences are real (e.g., the 1362 cm^{-1} peak), for the weak and poorly resolved bands we consider ±2 cm^{-1} to fall within the limits of detection error. Therefore, we do not report any significant frequency shifts for the bands in the low-frequency (∼200−500 cm^{-1}) region.

Figures 2 and 3 present the spectra of swelling mitochondria. Only the soluble form of cytochrome *c* is released when the mitochondria lose outer membrane integrity. A soluble (native) conformation of cytochrome *c* is characterized by the well-resolved octet of bands between 347 and 421 cm^{-1}. Examination of the dynamics of these bands reveals that the Raman spectra of swelling mitochondria in this region eventually attain a well-resolved eight-peak structure that was not observed in the intact mitochondria. We suggest that these changes reflect appearance of an increasing pool of free cytochrome *c* in the intermembrane space. The resonance Raman spectra of both bovine heart and rat liver mitochondria supernatants (the mitochondria preparations were fractioned after Ca^{2+} overload) in Figure 4 show a one-to-one correspondence with the spectrum of reduced cytochrome *c*. These results obviously demonstrate that cytochrome *c* released from mitochondria converts to its solution phase conformation. The spectra of mitochondria pellets in the low-frequency region (Figure 5 a) are quite similar to that of intact mitochondria, which suggests that some fraction of cytochrome *c* remains bound to the inner membrane, even after the mitochondria have ruptured.

Mid-Frequency Region Near 700 cm^{-1}. The Raman spectra of mitochondria in the mid-frequency region around 700 cm^{-1} exhibit more dramatic changes with respect to the solution phase cytochrome *c* spectrum. The main difference is the appearance of a strong band at 675 cm^{-1} that is absent in cytochrome *c* spectra. This band is more strongly enhanced in the spectrum of rat liver mitochondria. At this time, we are unable to make a firm assignment of this band and its dynamics during mitochondria swelling (Figure 2a,b). This band is absent in the spectrum of native cytochrome *c* and the mitochondria supernatants. It appears in the spectra of intact mitochondria and eventually vanishes as the mitochondria swell. Thus, it is conceivable that this band might signal interactions between the cytochrome *c* and the membrane lipids upon association. However, previous resonance Raman studies of the cytochrome *b*−*c* complex (*33*−*36*), cytochrome b_{562-O} (*52*), reduced mitochondria (*53*), and our own studies (Figure 7) demonstrate that the band at 675 cm^{-1} is a common feature of *b*-type hemes.

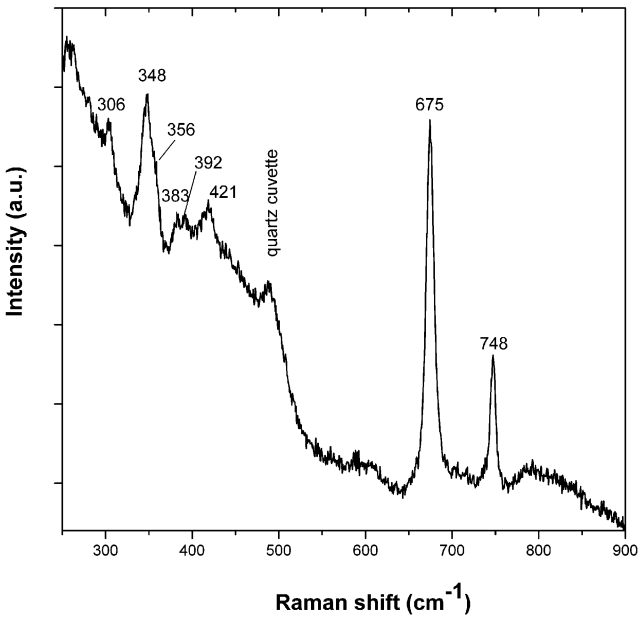

FIGURE 7: Resonance Raman spectrum of cytochrome b_5 in buffer solution obtained with 441.6 nm excitation.

The use of 413.1 nm excitation could be expected to provide conditions for selective resonance enhancement of the vibrational modes of reduced cytochrome *c* since its Soret peak is at 415 nm. However, this argument is effective only for the low-frequency modes. As shown previously (*54*, *55*), the Raman excitation profiles of cytochrome *c* display strong resonant enhancement up to one Raman quantum to the blue of the Soret band vibrational origin. The peak positions of the Soret bands of *b*-type cytochromes are red-shifted by 10−19 nm (500−1000 cm^{-1}) from 413.1 nm; thus, excitation at this wavelength will minimize the interference from low frequency Raman scattering of *b*-type hemes. On the other hand, the potential for relatively strong Raman scattering of high frequency *b*-type heme modes, along with the fluorescent background present in the experimental data (e.g., Figure 4b), does not allow us to quantitatively determine the contribution from *b*-type hemes in the high-frequency region of mitochondria (*33*−*36*). Therefore, on the basis of the available experimental data, it is difficult to unequivocally explain the dynamics of the 675 cm^{-1} mode during mitochondria swelling and protein release. However, it is likely that the observed spectral effects at 675 cm^{-1} can be attributed to *b*-type cytochromes and their transformations during mitochondrial swelling.

Another major discrepancy between the spectra of soluble cytochrome *c* and cytochrome *c* within the mitochondria is found in the region of the triplet centered near 692 cm^{-1}. In the Soret-excited spectrum of reduced cytochrome *c* there are three characteristic bands near 700 cm^{-1}: a strong broad band at 692 cm^{-1} and two resolved shoulders at 682 and at 700 cm^{-1}. The shoulder at 700 cm^{-1} was identified as the ν_7 stretching mode, and the 682 and 692 cm^{-1} bands were assigned to C−S stretching of the two thioether groups (*50*).

The complex structure of the bands near 700 cm^{-1} is lost in intact mitochondria spectra, and only one peak can be resolved at 688 cm^{-1}. In both bovine heart and rat liver

mitochondria spectra, the band at 688 cm^{-1} is weaker as compared to the band at 675 cm^{-1}; moreover, in the rat liver mitochondria spectrum the 688 cm^{-1} mode appears as a shoulder. However, the distribution of the amplitudes might be somewhat distorted because of a strong fluorescence background. The spectra of swelling bovine heart mitochondria do not show a noticeable shift of mode frequency, and the band at 688 cm^{-1} stays at the same position while the mitochondria undergo swelling and release of cytochrome *c*. The triplet structure of the bands centered at 692 cm^{-1} is not identifiable in the swelling bovine heart mitochondria. On the other hand, a clear triplet structure emerges in the spectrum of the bovine heart supernatant (Figure 4a), and the correlation between the Raman frequencies of the supernatant with the modes of soluble reduced cytochrome *c* is excellent (682, 692, and 700 cm^{-1}). The pellets from bovine heart mitochondria (Figure 5a) show a single 688 cm^{-1} band as found in intact and swelling mitochondria.

The spectra of swelling rat liver mitochondria display a somewhat different behavior in the 700 cm^{-1} region. When mitochondria undergo swelling and the 675 cm^{-1} mode intensity decreases, we can clearly see the development of a triplet structure near 692 cm^{-1}. The spectrum of rat liver mitochondria supernatant (Figure 4a) again is very similar to that of soluble reduced cytochrome *c*. The spectrum of rat liver pellets (Figure 5a) displays similarity with the intact mitochondria spectrum in the low-frequency region, but the structure of the bands near 700 cm^{-1} is slightly changed: the band at 688 cm^{-1} converts from a shoulder (Figure 1a) to a peak, and a weak shoulder is recognizable at 682 cm^{-1}.

Taken together, these data suggest that in the intact mitochondria a major part of cytochrome *c* molecules are in the membrane-bound conformation, and binding to the membrane causes alterations in the structure of the triplet bands near 692 cm^{-1}. The room temperature Soret-excited resonance Raman spectrum of native (soluble) ferrous cytochrome *c* has two clearly resolved thioether (C_a−S) stretching bands at 692 and at 682 cm^{-1}. At low temperature, the complex triplet envelope resolves into three distinct bands (*55*). Detailed analysis of the cytochrome *c* enhancement pattern (*50*) demonstrated that the cytochrome *c* $\pi-\pi^*$ excited-state undergoes a large expansion along coordinates that involve substantial (C_a−S) stretching. Because the (C_a−S) bonds attach the heme to the protein, binding to the membrane might perturb these linkages and affect the Raman intensity. Detachment of the protein from the membrane would restore the original solution structure of the protein. Therefore, one can observe the emerging triplet structure of the bands near 680−700 cm^{-1} during mitochondria swelling and the clear appearance of all three bands in the supernatant solution samples. The fact that the appearance of the triplet structure during swelling is noticeable only for rat liver mitochondria may be explained by the differences between the membrane structure in bovine heart and rat liver mitochondria. The membrane of bovine heart mitochondria contains many more cristae that are likely to retain cytochrome *c* during the swelling process so that less material is converted into the free solution phase.

Additional indirect evidence that cytochrome *c* is more easily released from swelling rat liver mitochondria comes from the absorption spectra of the supernatants (Figure 6). Although it is speculative to use the absorption spectra obtained under these conditions to provide quantative information about the concentration of the released cytochrome *c*, they do show qualitatively that the amount of released cytochrome *c* is higher for rat liver mitochondria. We used the same quantities of the two mitochondria preparations (about 3 mL) for pelleting, and the absorption spectra were measured in matched cuvettes (optical path is 3 mm). Figure 6 also presents the absorption spectrum of reduced cytochrome *c* in buffer solution. Comparison of the spectra in Figure 6 shows a good agreement between the absorption peak positions of the cytochrome *c* released from mitochondria and native ferrous cytochrome *c*.

High-Frequency Region. The inability to clearly resolve all of the high-frequency Raman modes of bovine heart and rat liver mitochondria limits the analysis. The high-frequency region (1200−1700 cm^{-1}) includes the oxidation, core-size, and spin marker bands ν_4, ν_3, ν_2, and ν_{10}. For these modes, correlations between frequencies and electronic configuration, core size, and ligation state of the heme iron are well-established (*49*). For reduced cytochrome *c*, these marker bands are located at 1362, 1492, 1592, and 1622 cm^{-1}, which are the positions expected for a 6-coordinate low-spin heme.

One of the spin state marker bands, ν_3, in mitochondria is found at 1493 cm^{-1}, which correlates well with native reduced cytochrome *c* and corresponds to the low-spin state (Figure 1b). The other spin-state marker is found at 1473 cm^{-1} and conceivably reflects the emergence of a pool of high-spin cytochromes. However, the *a*-type heme of cytochrome *c* oxidase also has a weak ν_{28} mode at 1472 cm^{-1} (*56*). The Soret band peak position of cytochrome *c* oxidase is found at 445 nm, and the resonance Raman spectra of intact reduced mitochondria, obtained by Adar and Erecinska (*57*) using the 441.6 nm HeCd laser line, show a weak band at 1472 cm^{-1}. A band at 1472 cm^{-1} was also resolved in the spectrum of soluble cytochrome *c* oxidase, excited at 413.1 nm (*31*). This band was slightly smaller with respect to the ν_3 mode of ferric cytochrome *c*, obtained under similar experimental conditions (Figure 5A,B in ref *31*). In our preparations, the cytochrome *c* oxidase concentration is calculated to be approximately 40 μM (the values for cytochrome content of isolated mitochondria are found in Table 4.7 of ref *1*). The cytochrome *c* concentration is found to be 30 μM for bovine heart and 10.6 μM for rat liver mitochondria, respectively. It is therefore possible, or even likely, that the weak 1472 cm^{-1} mode of cytochrome *c* oxidase is enhanced sufficiently at 413.1 nm to become visible relative to the 1493 cm^{-1} mode of ferrous cytochrome *c* as observed in the mitochondria spectra of Figure 1b.

The oxidation state marker band ν_4 is downshifted in mitochondria by 2 cm^{-1}. In reduced cytochrome *c*, this band has a small shoulder at 1397 cm^{-1} (Figure 1b) that is also downshifted in mitochondria to 1393 cm^{-1}. The positions of ν_4 and the shoulder in supernatant preparations are found at 1362 and 1398 cm^{-1}, which are the same as in native cytochrome *c*. In the pellet preparations of bovine heart and rat liver mitochondria, ν_4 is found at 1362 cm^{-1}. An upshift of ν_4 or the appearance of a shoulder at 1372 cm^{-1}, if observed, would indicate a change from the fully reduced state to one with an oxidized population of cytochromes (the oxidized cytochrome *c* has ν_4 at 1372 cm^{-1}). We do not observe such changes; thus, the cytochrome *c* remains in the fully reduced state. The downshift of ν_4 by 2 cm^{-1} is

assigned to perturbations associated with the protein−membrane interaction. The behavior of this band during mitochondria swelling and cytochrome *c* release gives support to the hypothesis that the changes are due to protein intercalation in the inner membrane. We note that ν_4 in rat liver and bovine heart pellets (Figure 5b) remains at 1360 cm^{-1} as found for intact mitochondria, while in both supernatants this mode is observed at 1362 cm^{-1} similar to native cytochrome *c*. Therefore, some fraction of cytochrome *c* remains in the bound conformation within the membrane remnants formed after mitochondria swelling and centrifugation. This observation is in agreement with the estimation of Cortese et al. (*22*), who reported that approximately 11% of cytochrome *c* remains bound to inner mitochondria membrane at ionic strength ~150 mM.

The ν_2 band at 1592 cm^{-1} is not clearly resolved in mitochondria spectra, but we do detect a shoulder at 1623 cm^{-1}, which can be assigned to the ν_{10} mode. These spectral features are consistent with the heme in mitochondria being in a ferrous low-spin state.

Unambiguous assignments of the bands observed in the mitochondria spectra at 1245, 1523, 1568, and 1612 cm^{-1} are intricate in the absence of additional information. These bands are not spectral features of native cytochrome *c*. They also were not detected in the spectra of purified cytochrome b_5 (*33*, *34*) and cytochrome b_{566} (*35*) at Q-band excitation (except 1612 cm^{-1}, which is very weak in the cytochrome b_{566} spectrum with 568.7 nm excitation (*35*)). However, some of these bands (a weak shoulder at 1568 $cm^{-1}$and a well-resolved band at 1610 cm^{-1}) were observed in mitochondria spectra with 441.6 nm excitation, which provides preferable enhancement for cytochrome *c* oxidase and indicates that this species also contributes weakly to the Raman spectra obtained using 413 nm excitation.

In summary, these experiments reveal that the changes in protein conformation that were previously reported when cytochrome *c* binds to artificial (*15*−*21*, *28*−*47*) and natural (*22*, *23*) membrane systems are qualitatively similar to the transformations that occur when cytochrome *c* is attached to the inner mitochondria membrane. This gives support to the idea that protein−phospholipid model systems provide an important and reliable test bed for studies of protein−membrane interactions. Cytochrome *c* molecules in mitochondria are found primarily in the membrane-bound state, and binding evidently causes a partial opening of the heme pocket and alteration of the heme-Cys14 and heme-Cys17 thioether bonds. As mitochondria swell, a significant pool of free (solution phase) cytochrome *c* is created through detachment of the protein from the membrane. This pool is released once the outer membrane is permeabilized. Also, there is a portion of the cytochrome *c* that remains bound to the inner membrane even after the mitochondria are overloaded with Ca^{2+} and swell to the breaking point. This signifies the existence of a tightly bound protein fraction. Finally, the experimental data (i.e., the dynamics of the 675 cm^{-1} mode) suggest that not only cytochrome *c*, but also the cytochrome *b* proteins, undergo transformation as the outer membrane is altered during mitochondrial swelling and rupture.

Overall, this paper addresses key spectroscopic aspects of cytochrome *c* binding to mitochondrial membranes. Cytochrome *c* undergoes a conformational change early in apoptosis and necrosis, which is not due to a covalent modification but is consistent with a membrane association induced transformation (*23*). The release of cytochrome *c* from its membrane bound state in the mitochondria is a fundamental signaling mechanism for cell death. The ability to understand and control the process of cytochrome *c* binding and release from the mitochondrial membrane would likely have significant ramifications in our ability to treat human cancer cells, many, if not all of which, display a strong resistance to apoptosis (*58*).

ACKNOWLEDGMENT

We thank David Wharton for general advice and Ted Sjodin for his help in the Raman experiments, particularly those involving cytochrome b_5.

REFERENCES

1. Tyler, D. (1992) *The mitochondrion in health and disease*, VCH Publishers, New York.
2. Green, D. R., and Reed, J. C. (1998) *Science 282*, 1309−1312.
3. Pettigrew, G. W., and Moore, G. R. (1987) *Cytochrome c—Biological Aspects*, Springer-Verlag, Berlin.
4. Scorrano, L., Ashiya, M., Buttle, K., Weiler, S., Oakes, S. A., Mannella, C. A., and Korsmeyer, S. J. (2002) *Developmental Cell 2*, 55−67.
5. Nicholls, P., Mochan, E., and Kimelberg, H. K. (1969) *FEBS Lett. 3*, 242−246.
6. Woitczak, L., and Sottocasa, G. L. (1972) *J. Membr. Biol. 7*, 313−324.
7. Nickolls, P. (1974) *Biochem. Biophys. Acta 346*, 261−310.
8. Matlib, M. A., and O'Brien, P. J. (1976) *Arch. Biochem. Biophys. 173*, 27−33.
9. Salemne, F. R. (1977) *Annu. Rev. Biochem. 47*, 299−329.
10. Jasaitis, A. A., and Krivichiene, Z. J. (1980) *European Bioenergetics Conference Reports*, Vol. 1, p 111−112 (Patron, Ed.) Italian Bioenergetics and Biomembranes Group, University of Bologna, Italy.
11. Bernardi, P., and Azzone, G. F. (1981) *J. Biol. Chem. 256*(14), 7187−7192.
12. Wohlrab, H. (1970) *Biochemistry 9*, 474−479.
13. Rodriguez-Maranon, M. J., Qiu, F., Strak, R. E., White, S. P., Zhang, X., Foundling, S. I., Rodriguez, V., Schilling, C. L., Bunce, R. A., and Rivera, M. (1996) *Biochemistry 35*, 16378−16390.
14. Hom, K., Ma, Q. F., Wolfe, G., Zhang, H., Storch, E. M., Daggett, V., Basus, V. J., and Waskell, L. (2000) *Biochemistry 39*, 14025−14039.
15. Spooner, P. J. R., and Watts, A. (1991) *Biochemistry 30*, 3880−3885.
16. Spooner, P. J. R., and Watts, A. (1992) *Biochemistry 31*, 10129−10138.
17. Heimburg, T., Hildebrandt, P., and Marsh, D. (1991) *Biochemistry 30*, 9084−9089.
18. Heimburg, T., Hildebrandt, P., and Marsh, D. (1990) *Europ. Biophys. J. 18*, 193−201.
19. Soussi, B., Bylund-Fellenius, A.-C., Schersten, T., and Angstrom, J. (1990) *Biochem. J. 265*, 227−232.
20. Pinheiro, T. J. T., Elove, G. A., Watts, A., and Roder, H. (1997) *Biochemistry 36*, 13122−13132.
21. de Jongh, H. H., Killian, J. A., and de Kruijff, B. (1992) *Biochemistry 31*, 1634−1643.
22. Cortese, J. D., Voglino, L. A., and Hackenbrock, C. R. (1998) *Biochemistry 37*, 6402−6409.
23. Jemmerson, R., Liu, J., Hausauer, D., Lam, K. P., Mondino, A., and Nelson, R. D. (1999) *Biochemistry 38*, 3599−3609.
24. Rytomaa, M., Mustonen, P., and Kinnunen, P. K. J. (1992) *J. Biol. Chem. 267*, 22243−22248.
25. Rytomaa, M., and Kinnunen, P. K. J. (1995) *J. Biol. Chem. 270*, 3197−3202.
26. Tuominen, E. K., Zhu, K., Wallace, C. J. A., Clark-Lewis, I., Craig, D. B., Rytomaa, M., and Kinnunen, P. K. J. (2001) *J. Biol. Chem. 276*(22), 19356−19362.
27. Tuominen, E. K., Wallace, C. J. A., and Kinnunen, P. K. J. (2002) *J. Biol. Chem. 277*, 8822−8826.

28. Nantes, I. L., Zucchi, M. R., Nasciemento, O. R., and Faljoni-Alario, A. (2001) *J. Biol. Chem. 276*(1), 153−158.
29. Gorbenko, G. P. (1999) *Biochem. Biophys. Acta 1420*, 1−13.
30. Witt, H., Zickermann, V., and Ludwig, B. (1995) *Biochem. Biophys. Acta 1230*, 74−76.
31. Dopner, S., Hildebrandt, P., Rossel, F. I., Mauk, A. G., Walter, M., Buse, G., and Soulimane, T. (1999) *Europ. J. Biochem. 261*, 379−391.
32. Ott, M., Robertson, J. D., Gogvadze, V., Zhivotovsky, B., and Orrenius, S. (2002) *PNAS 99*, 1259−1263.
33. Adar, F., and Erecinska, M. (1974) *Arch. Biochem. Biophys. 165*, 570−580.
34. Adar, F., and Erecinska, M. (1975) *Arch. Biochem. Biophys. 170*, 644−650.
35. Adar, F., and Erecinska, M. (1977) *FEBS Lett. 80*, 195−199.
36. Adar, F., and Erecinska, M. (1978) *Biochemistry 17*, 5484−5488.
37. Wohlrab, H. (1969) *Biochem Biophys. Res. Commun. 35*, 560−564.
38. Joshi, S., and Sanadi, D. R. (1979) *Methods Enzymol. 55F*, 384−391.
39. Frey, T. G., and Mannella, C. A. (2000) *Trends Biochem. Sci. 25*, 319−324.
40. Hildebrandt, P., and Stockburger, M. (1989) *Biochemistry 28*, 6710−6728.
41. Hildebrandt, P. (1990) *Biophys. Acta 1040*, 175−186.
42. Spooner, P. J. R., and Watts, A. (1991) *Biochemistry 30*, 3871−3879.
43. Weber, B. M., and Bosshard, H. R. (1987) *PNAS USA 84*, 6687−6691.
44. Chottard, G., Michelon, M., Hervé, M., and Hervé, G. (1987) *Biochim. Biophys. Acta 916*, 402−410.
45. Muga, A., Mantsch, H. H., and Surewicz, W. K. (1991) *Biochemistry 30*, 2629−2635.
46. Antalík, M., Bona, M., and Kuchár, A. (1992) *Biochim. Biophys. Acta 1100*, 155−159.
47. Heimburg, T., and Marsh, D. (1993) *Biophys. J. 65*, 2408−2417.
48. Salamon, Z., and Tolin, G. (1996) *Biophys. J. 71*, 848−857.
49. Spiro, T. G. in *Iron Porphyrins* (1983) Part 2, Ch. 3, Addison-Wesley, Reading, MA.
50. Hu, S., Morris, I. K., Singh, J. P., Smith, K. M., and Spiro, T. G. (1993) *J. Am. Chem. Soc. 115*, 12446−12458.
51. Yeh, S. R., Takahashi, S., Fan, B., and Rousseau, D. L. (1997) *Nature Struct. Biol. 4*, 51−56.
52. Uno, T., Nishimura, Y., Tsuboi, M., Kita, K., and Anraku, Y. (1985) *J. Biol. Chem. 260*, 6755−6760.
53. Takahashi, T., and Ogura, T. (2002) *Bull. Chem. Soc. Jpn. 75*, 1001−1004.
54. Champion, P. M., and Albrecht, A. C. (1979) *J. Chem. Phys. 71*, 1110−1121.
55. Schomacker, K., Bangcharoenpaurpong, O., and Champion, P. M. (1984) *J. Chem. Phys. 80*, 4701−4717.
56. Spiro, T. G., Ed. (1988) *Biological Application of Resonance Raman Spectroscopy*, Wiley, New York.
57. Adar, F., and Erecinska, M. (1979) *Biochemistry 18*, 1825−1829.
58. Li, C., and Thompson, C. (2002) *Science 298*, 1346−1347.

BI027387Y